Eur. Phys. J. A **37**, 9–14 (2008)
DOI 10.1140/epja/i2008-10604-8

THE EUROPEAN PHYSICAL JOURNAL A

Regular Article – Experimental Physics

# Neutron velocity distribution from a superthermal solid $^2H_2$ ultracold neutron source

I. Altarev[3], M. Daum[4,a], A. Frei[3], E. Gutsmiedl[3], G. Hampel[1], F.J. Hartmann[3], W. Heil[2], A. Knecht[4,b], J.V. Kratz[1], T. Lauer[1], M. Meier[4], S. Paul[3], U. Schmidt[5], Y. Sobolev[1,c], N. Wiehl[1], and G. Zsigmond[4]

[1] Institut für Kernchemie, Johannes Gutenberg-Universität, Fritz-Strassmann-Weg 2, D-55128 Mainz, Germany
[2] Institut für Physik, Johannes Gutenberg-Universität, Staudingerweg 7, D-55128 Mainz, Germany
[3] Physik-Department, Technische Universität München, James-Franck-Strasse, D-85748 Garching, Germany
[4] PSI, Paul Scherrer Institut, CH 5232 Villigen PSI, Switzerland
[5] Physikalisches Institut, Ruprecht-Karls-Universität, Heidelberg, Germany

Received: 3 March 2008 / Revised: 21 May 2008
Published online: 7 July 2008 – 
Communicated by P. Braun-Munzinger

**Abstract.** We have determined for the first time the velocity distribution of neutrons from a solid $^2H_2$ ultracold neutron (UCN) source. The spectrum rises sharply above 4.5 m/s and has a maximum around 7 m/s after transport in an 8 m long guide. The number of neutrons in the UCN velocity range ($< 7$ m/s) may be increased by a factor of two by placing the experiment 1 m above the UCN source level.

**PACS.** 29.25.Dz Neutron sources – 28.20.Gd Neutron transport: diffusion and moderation

## 1 Introduction

Ultracold neutrons (UCN) have energies below $\sim 350$ neV, *i.e.* temperatures below a few millikelvin, and can be stored [1–3] i) in material bottles through the averaged or coherent strong-interaction potential of materials, $V_f$; this potential is, *e.g.*, 352 neV for diamond, 345 neV for $^{58}$Ni, 248 neV for Be, and 190 neV for stainless steel [4]; ii) in magnetic bottles through the electromagnetic interaction with the neutron magnetic moment, $dV_m/dB = 60\,\text{neV} \cdot \text{T}^{-1}$, and iii) using the gravitational field of the Earth as confinement, $V_g = m \cdot g \cdot h$, $dV_g/dh = 102\,\text{neV} \cdot \text{m}^{-1}$. Combinations of these three interactions have been used successfully for the storage of UCN, see, *e.g.*, refs. [5, 6]. Because of their long observation times, stored neutrons play an increasing role in measurements of fundamental properties of the neutron, such as the electric dipole moment (or its upper limit) [7], the lifetime of the free neutron [8, 9], and the gravitational interaction [10]. The UCN densities provided by existing reactor sources, however, limit the precision of these basic experiments.

At present, several projects aim at building new sources of ultracold neutrons in order to provide the required increase in intensity for significant improvements in the experiments. Two source types having the potential to produce substantially higher UCN densities are being pursued, based on non-equilibrium moderator systems, using either superfluid helium [11–14] or solid $^2H_2$ [15–20] to downscatter (convert) thermal and cold neutrons. These new sources have —in principle— the potential to reach UCN densities higher by more than two orders of magnitude over todays most intense UCN source at the ILL in Grenoble, France [21].

## 2 Superthermal solid $^2H_2$ UCN source

A prototype of an UCN source with a solid $^2H_2$ converter [19] at $\sim 6$ K has been set up at the TRIGA Mark II reactor [22,23] of the Mainz University. This reactor can be operated at a steady-state power of 100 kW or in pulsed mode with a maximum power of 250 MW and an energy release of 10 MW [24]. Detailed reports on the UCN source principle and first measurements of the source parameters and performance have been published elsewhere [25]. The work described here is concerned with the extraction of UCN from the solid $^2H_2$ converter at this new source. In such a cold, superthermal moderator (converter), thermal or cold neutrons are downscattered into the ultracold neutron range ($E_{kin} < 350$ neV) by inelastic scattering, where the energy is transferred to create phonons in the converter crystal. The resulting heat transfer to the converter material is compensated by forced cooling with liquid helium.

[a] e-mail: manfred.daum@psi.ch
[b] *Also at* Physics Department, University Zürich, Switzerland.
[c] *On leave from* Petersburg Nuclear Physics Institute, Gatchina, Russia.

The thickness of solid $^2H_2$ converters is chosen such that neutrons can leave it after being downscattered to UCN energies. At those energies, the lifetime of neutrons in solid $^2H_2$ depends on the quality and geometry of the crystal and is about 30–80 ms [16,17,26,27]. When leaving the converter, the neutrons are accelerated by the coherent strong-interaction potential of the material, the so-called material optical potential [28–31], $V_f = V - iW$. The potential parameters $V$ and $W$ depend on the nuclear properties of the surface atoms, $V = (2\pi\hbar^2/m) \cdot N \cdot b$ and $W = (\hbar/2) \cdot N \cdot \sigma \cdot v$. Here, $m$ and $v$ denote the mass of the neutron and its velocity, respectively, $N$ the atom number density, $b$ the bound coherent nuclear scattering length and $\sigma$ the cross-section for neutron loss (absorption and up-scattering). The real part of the potential, $V$, defines the height of the potential, the imaginary part, $W$, the absorption loss. Thus, neutrons from a solid $^2H_2$ converter are expected to have energies above the respective material optical potential, $V = 105$ neV [4], corresponding to a velocity of 4.5 m/s.

## 3 Experimental setup

We have determined the velocity distribution of neutrons from the solid $^2H_2$ UCN source at the TRIGA Mainz with the time-of-flight (TOF) method. In principle, a TOF measurement can be performed both in the pulsed or in the steady-state mode of the reactor. In the pulsed mode, the minimal overall length of the flight path is from the geometrical layout (shielding, cryostat, etc., cf. [25]) more than 6 m. In such a long UCN guide, part of the neutrons are repeatedly diffusely scattered back and forth and the neutron guide acts also as a neutron storage chamber. This leads to a delay of these scattered neutrons in reaching the detector apparently at a lower velocity. In the steady-state mode using a chopper for the TOF information, the TOF path length can be chosen to be much shorter, see below.

In this experiment, the reactor was operated in the steady-state mode at 100 kW. The amount of $^2H_2$ frozen in the UCN converter was i) 4 mole and ii) 6.1 mole corresponding to a converter thicknesses of about 2.4 cm and 3.6 cm, respectively, assuming a purely cylindrical shape of the converter crystal. The 4 mole crystal was carefully thermally cycled (cf. [25]) for optimal UCN yield and the neutron counts in the pulsed mode [25] were reproduced before switching to the steady-state mode at 100 kW. The 6.1 mole crystal was mainly used for the precise time calibration of the system: The UCN yield is lower when the crystal is not optimized and the relative yield of neutrons with velocities higher than $\sim 7$ m/s is increased, see below. These neutrons are better suited for time calibration because of their lower diffuse reflection probability and their narrower angular distribution in the forward direction.

Neutrons can leave the $^2H_2$ converter horizontally in electropolished stainless-steel tubes of 66 mm inner diameter from the tangential port C of the reactor [25] to the detector. Outside the biological shield of the reactor core, at a distance of $\sim 4$ m from the solid $^2H_2$ converter, the in-pile part of the neutron guide is terminated by an aluminium window at room temperature. Behind this, the neutron beam has a horizontal bend of 45° in order to avoid direct view to the reactor core and to reduce the background from thermal and epithermal neutrons. Finally, a 1.5 m long straight neutron guide has been installed.

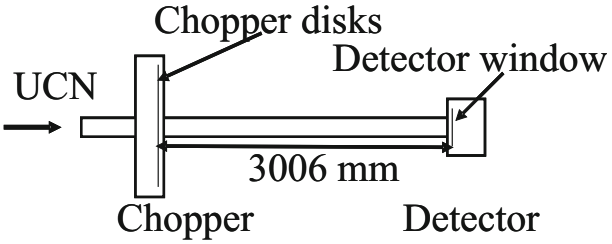


**Fig. 1.** Sketch of the experimental setup for the time-of-flight experiment with a chopper.

For the correct determination of a velocity distribution with the TOF method, we assume a high guide transmission for UCN, *i.e.* a high percentage of specular reflections in the UCN guide system, which is experimentally supported by ref. [32]. The experimental setup for the TOF measurement, described in refs. [33–35], is installed behind this neutron guide; a sketch is shown in fig. 1. Slow neutrons enter the apparatus at a rate of $\sim 650\,s^{-1}$ ($\sim 850\,s^{-1}$ for the 6.1 mole crystal) and pass through a chopper operating with a duty cycle of 5.5% [33]. They are registered in a neutron detector with 18 hPa $^3$He and 12 hPa $CO_2$ in about 1070 hPa Ar. This detector was installed directly behind the TOF path. The Al entrance window of the detector was 0.1 mm thick with an energy barrier of 54 neV from the material optical potential of aluminium and caused some reduction of the detector efficiency. With this setup, the (averaged) velocity component along the forward direction can be measured [34,35].

## 4 Data acquisition

As DAQ system we used the PCI-BUS module MCD-2 (dual imput multiscaler, FAST ComTec). The start signal for the TOF spectra was delivered from the chopper control unit. For the event (stop) signal, the discriminator output of a Canberra 2015 Amplifier with intergrated single-channel analyser was used. The discriminator level was adjusted well above the noise level of the detector signal. The dwell time for the multiscaler was 2.5 ms.

In total, eight different TOF spectra were recorded, two for the 4 mole crystal and six for the 6.1 mole crystal: we took data at three different chopper rotation frequencies, 1.00 Hz, 0.75 Hz, and 0.50 Hz, and at two TOF paths from the chopper disks to the detector. The TOF paths, $l_l = (3016 \pm 5)$ mm and $l_s = (1616 \pm 5)$, are the sum of i) the tube lengths, 3000 mm and 1600 mm, respectively; ii) the distance from the chopper disks to the beginning of the tube as well as that from the end of the tube to the detector entrance window, 3 mm each; and iii) the mean free path of UCN with velocities between 4.5 m/s and 7 m/s in the $^3$He detector, on average 10 mm. The

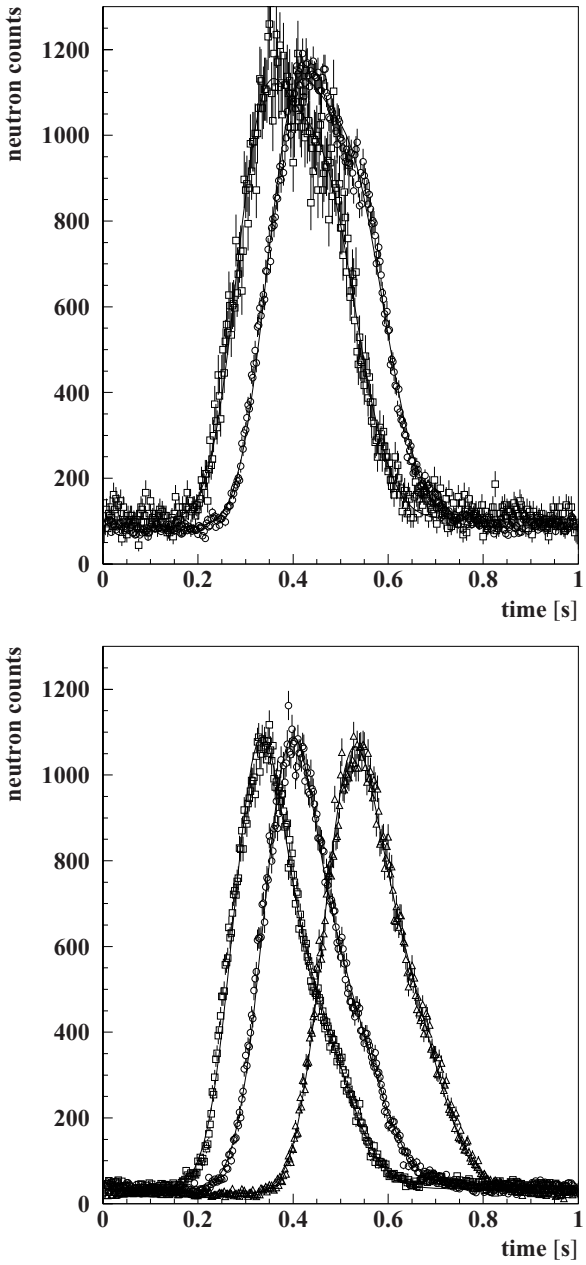


**Fig. 2.** Time-of-flight spectra for a flight path of 1.616 m. Top: converter volume of 4 mole, chopper frequencies of 1.00 Hz (open squares) and 0.75 Hz (open circles). Bottom: converter volume of 6.1 mole, chopper frequencies of 1 Hz (open squares), 0.75 Hz (open circles) and 0.50 Hz (open triangles). Two Gaussians and a flat background were fitted to each of the data sets (solid lines). The time spectra at different chopping frequencies have to be corrected by a frequency-dependent time offset, see text.

distance uncertainties originate mainly from the different path lengths of the neutrons in the detector, *i.e.* the position of the detection reaction ($n+^3He \rightarrow {}^3H+p$). Figure 2 shows the TOF spectra taken at a flight path of 1.616 m with the 4 mole source at chopper frequencies of 1.00 Hz and 0.75 Hz and with the 6.1 mole source for all three chopper frequencies.

### 4.1 Time-of-flight calibration

Time calibration of the system was obtained by comparing i) at one distance the spectra taken at two different chopper frequencies; ii) at one chopper frequency the TOF spectra taken at the two distances. We obtained eight partially dependent calibration measurements by comparing the TOF spectra at different chopper frequencies, three pairs at each distance: a) 1.00 Hz, 0.75 Hz, b) 1.0 Hz, 0.50 Hz, and c) 0.75 Hz, 0.50 Hz, and additional three calibration measurements (one per frequency) by comparing the TOF spectra at the two distances.

In all eight TOF spectra, two Gaussians and a flat background were fitted to the data, see, *e.g.*, fig. 2. This procedure results in a suitable parameterization of the experimental data. The $\chi^2$ per degree of freedom of the fits were in all cases between 1.1 and 1.9. These values reflect the rather simplified parameterization of the spectra by two Gaussians.

With the time calibration using different chopper frequencies, *e.g.*, 1.00 Hz and 0.75 Hz at 1.6 m flight path, we find for the time of the first Gaussian peak in the 0.75 Hz data $t + 1.33 \cdot \delta t = (0.390 \pm 0.003)$ s and $t + \delta t = (0.330 \pm 0.007)$ s at 1.00 Hz, cf. fig. 2. Here, $\delta t$ is the time difference between the electronic trigger signal from the chopper and its real opening time [33] for a chopper frequency of 1 Hz. Since the electronic signal is produced by a photoelectric barrier triggered by an interrupter on one of the rotating chopper discs, the value of $\delta t$ depends on the chopper frequency. The factor 1.33 $[= (1\,\text{Hz})/(0.75\,\text{Hz})]$ in front of the parameter $\delta t$ originates from the normalization of $\delta t$ to 1 Hz. Thus, from the above numbers, we get $0.33 \cdot \delta t = (0.060 \pm 0.0076)$ s and therefore $\delta t = (0.180 \pm 0.022)$ s. Similar and partially more precise values for $\delta t$ are obtained from the 6.1 mole data and from the calibration for each frequency at two distances. Averaging all available and independent information we find $\delta t(1\,\text{Hz}) = (0.191 \pm 0.003)$ s (four independent measurements) from evaluating $\delta t$ from the different frequencies at the two distances (method 1), and $\delta t(1\,\text{Hz}) = (0.192 \pm 0.007)$ from evaluating at one distance the different frequencies (method 2). These values were obtained from a fit with i) a $\chi^2$ per degree of freedom of 0.7 for method 1, corresponding to a confidence level of 0.45, and ii) a $\chi^2$ per degree of freedom of 0.3 for method 1, corresponding to a confidence level of $\sim 0.8$.

## 5 Data analysis

### 5.1 Deconvolution of the TOF spectra

The deconvolution of the TOF spectra and the conversion into velocity distributions were performed in several steps. Firstly, and in order to obtain smooth functions before the deconvolution, we used the above-mentioned two-Gaussian fit to the data with a constant background, see fig. 2. After the fit, the background was subtracted: in fig. 2 (top), the fitted background per channel was $(86.7 \pm 1.1)$ for the 0.75 Hz data and $(104 \pm 3)$ for the

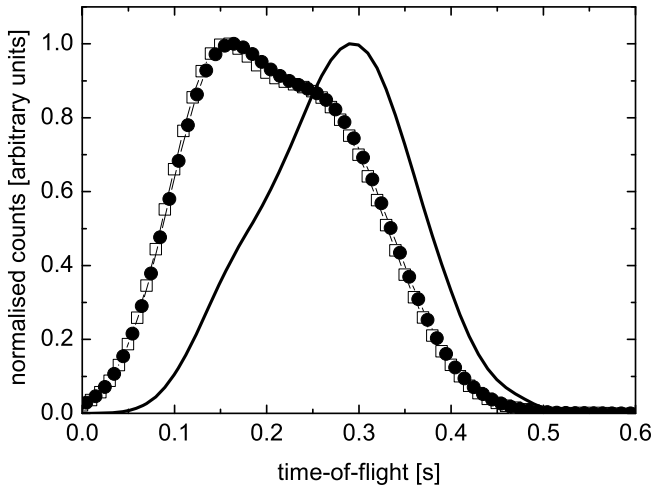


**Fig. 3.** Deconvoluted time-of-flight spectra after background subtraction for a flight path of 1.6 m. The bin width is 2.5 ms. Squares: chopper frequency 0.75 Hz; full dots: chopper frequency 1.00 Hz. The conversion from the TOF distribution to a velocity distribution parallel to the guide axis includes multiplication of the data by the derivative $|\mathrm{d}t/\mathrm{d}v_\mathrm{p}| = t^2/d$, see the solid line.

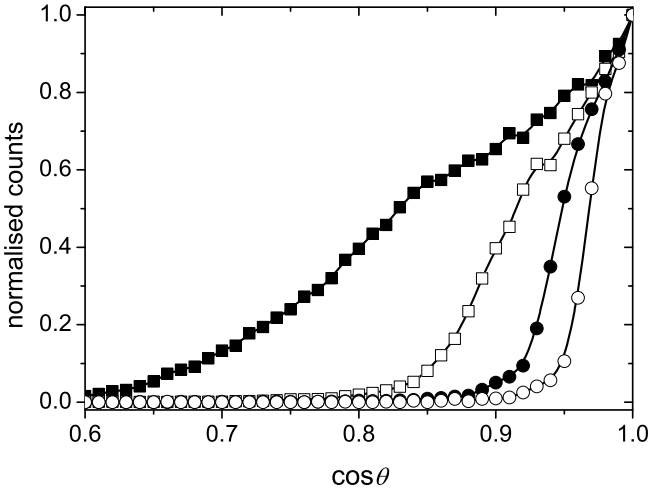


**Fig. 4.** Simulated distribution of the polar angle $\theta$ between the flight direction of the neutrons and the axis of the neutron guide. The total flight path from the source to the detector is 7.1 m corresponding to the short distance between the chopper and the detector, $l_\mathrm{s} = 1.616$ m; Velocity intervals shown: full squares 5–10 m/s, open squares 10–15 m/s, full circles 15–20 m/s, open circles 20–25 m/s.

1.00 Hz data. In the next step, the time offsets, $\delta t(\nu_i)$, of the chopper corresponding to the two respective frequencies $\nu_i$ were subtracted. Then, the fitted corrected TOF spectra at 0.75 Hz and at 1.00 Hz were deconvoluted with the chopper resolution functions [33] which were approximated by rectangular time functions of widths 0.0733 s and 0.055 s for 0.75 Hz and 1.00 Hz, respectively.

The convolution of the two functions can be formulated in a discrete way as

$$f_i = \sum_j R_{ij} \cdot F_j \,,$$

where $R_{ij} = R(t_i - t_j)$ is the matrix form of the chopper resolution function, $F_j = F(t_j)$ is the set of UCN flight times in the bin $t_j + \Delta t$ with the dwell time $\Delta t = 0.0025$ s, and $f_i = f(t_i)$ are the measured UCN counts as obtained from the two-Gaussian fits. The deconvolution was performed as multiplication of the measured signal represented as $f_j = f(t_j)$ with the inverse matrix which corresponds to the resolution function

$$F_i = \sum_j R_{ij}^{-1} \cdot f_j \,.$$

The resulting deconvoluted TOF spectra for the two different chopper frequencies can be seen in fig. 3: the two spectra show excellent agreement. The data represent the neutron event distribution $\mathrm{d}N/\mathrm{d}t$. In order to obtain a velocity distribution $\mathrm{d}N/\mathrm{d}v_\mathrm{p}$ parallel to the guide axis, we performed the following steps: i) we multiplied the data with the derivative $|\mathrm{d}t/\mathrm{d}v_\mathrm{p}| = t^2/d$, where $d$ is the flight path; the result, normalized to arbitrary units, is shown as a solid line in fig. 3; ii) we converted the TOF axis to $v_\mathrm{p} = d/t$.

### 5.2 Absolute velocity distribution

The distribution of the absolute velocity $v = v_\mathrm{p}/\cos\theta$ was calculated from the measured distribution $v_\mathrm{p}$, and the $\theta$-distribution obtained from MC simulations. Here, $\theta$ is the polar angle between the guide axis and the neutron momentum vector. We used the VITESS neutron optics software [36,37] extended for UCN. The model parameter for completely diffuse reflections (cf. ref. [31], p. 100) was chosen to 4% per bounce for neutron velocities up to 6 m/s as deduced from MC modelling of purely UCN transmission measurements with about 96% per meter [38] for the stainless-steel guides in use. For higher velocities, we chose 1% diffuse reflection, as obtained from routine transmission measurements [39]. The distribution in $\theta$ is correlated with the parallel velocity component, see fig. 4. Finally, by randomly sampling the distribution in $v_\mathrm{p}$ and that in $\theta$, the absolute velocity distribution in $v$ was computed.

The absolute velocity spectrum of UCN is shown in fig. 5. Neutrons with transverse velocity components below 3.2 m/s cannot penetrate the aluminium entrance window of the detector due to the aluminium material optical potential of 54 neV [4], however, there are only very few events below 4.5 m/s. The velocity distribution rises sharply above this velocity and has a maximum around 7 m/s. Beyond the maximum, the neutron yield decreases approximately exponentially. The few neutrons with apparent velocities below 4.5 m/s are unexpected because of neutron acceleration at the surface of the cold $^2H_2$ converter with a material optical potential of 105 neV [4,40]. A detailed MC simulation showed that the probability of diffuse reflection in the UCN guide behind the chopper and reflections of neutrons with small perpendicular velocity components at the detector entrance window causes delay effects in the time-of-flight spectra. As a consequence, we

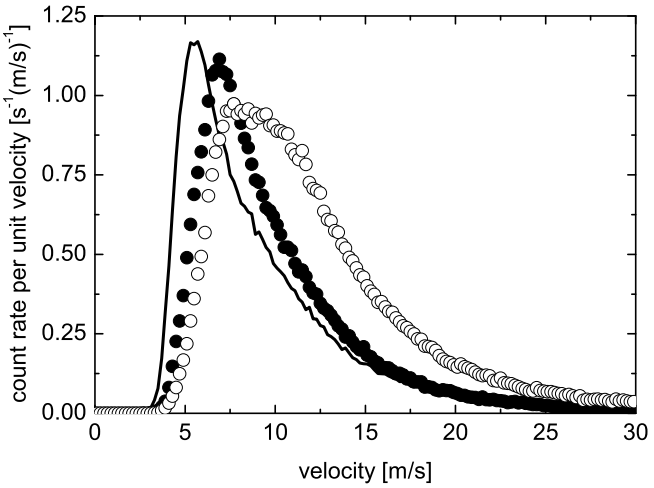


**Fig. 5.** Neutron velocity distribution from the superthermal solid $^2H_2$ ultracold neutron source at TRIGA Mainz. Full dots: data from the optimized 4 mole source. The line represents the velocity component parallel to the neutron beam axis. Open circles: data from the (not optimized) 6.1 mole source.

obtain an additional small fraction of UCN with apparently smaller energy than the boost energy of the solid $^2H_2$ converter.

The effect of a lower threshold for the velocity of neutrons leaving a solid deuterium UCN converter has been recently reported [40]. In that experiment, neutrons had to overcome a U-shaped neutron guide as a gravitational barrier. Besides energy selection by gravitation, the U-shaped neutron guide (with four 90° bends) acted also as a strong filter selecting preferentially neutrons with velocities below the critical velocity of the guide walls. In the present work, the filter effect of the neutron guides used is much less, thus allowing also transport of so-called "very cold neutrons" (VCN, with velocities higher than the critical velocity of the neutron guides), as can be seen from the measured TOF spectra.

From the 4 mole data shown in fig. 5, we obtain a fraction of UCN in the total neutron flux of $(25 \pm 6)\%$ (in this setup equivalent to $\sim 200$ UCN/s) and $(13 \pm 3)\%$ for the (non-optimized) 6.1 mole crystal (in this setup equivalent to $\sim 750$ VCN/s), respectively. These rates are in fair agreement with theoretical expectations [18, 26]. Please note that with more elaborately optimized source parameters, including, *e.g.*, a mesitylen premoderator, significantly higher rates have been obtained [25]. The uncertainty is dominated by that one originating from the diffuse-scattering parameter. By varying this parameter (between 1% and 4% per bounce), we obtain slightly different velocity distributions: the fraction of UCN is increased to 30% for the 4 mole crystal (16% for the 6.1 mole crystal) for a diffuse-scattering probability of 1% per bounce. The differences (1% *vs.* 4% diffuse scattering) are introduced as systematic uncertainties.

The obtained UCN yield (25%) differs a little from the one reported earlier [25] mainly because of a slightly different experimental setup: Firstly, in ref. [25], the neutrons were guided downwards by 0.6 m after a 90° bend for optimal penetration of the Al detector foil. In our setup, we avoided spectral shifts originating from an acceleration in the gravitational field of the earth. The additional 90° bend in ref. [25] obviously favoured the transport of neutrons with energies below the material optical potential of the stainless-steel neutron guides (190 neV corresponding to 6.0 m/s). Secondly, the detector used in ref. [19] was a GEM detector [41] with a slightly different detection efficiency.

From fig. 5, we learn that we can achieve an optimal storage yield of UCN by guiding the neutrons upwards by about 1 m, *i.e.* shifting the neutron spectrum down in energy due to deceleration by gravitation. Then, the neutron distribution between 5 m/s and 9 m/s is shifted into the UCN velocity range (0–7 m/s) that can be stored in a storage vessel with a wall coating of $\sim 250$ neV material optical potential corresponding to those of, *e.g.*, beryllium or diamond-like carbon [5, 6, 42]. With this procedure, we obtain an overall UCN gain of a factor of $\sim 2$, cf. fig. 5.

## 6 Conclusion

In conclusion, we have measured the velocity distribution of neutrons from the superthermal solid $^2H_2$ ultracold neutron source at the TRIGA Mark II reactor of Mainz University using a chopper and the time-of-flight method: i) The neutron spectrum rises sharply above 4.5 m/s. After transport in an 8 m stainless-steel neutron guide, the distribution has a maximum around 7 m/s, corresponding to $\sim 250$ neV, and decreases approximately exponentially above this velocity. ii) The yield of neutrons with velocities below the coherent strong-interaction potential of $^2H_2$ (105 neV) corresponding to a lower velocity limit of 4.5 m/s is very small and can be explained by diffuse, *i.e.* non-specular, scattering where the neutron guide can also be considered as an UCN storage chamber. iii) The number of storable neutrons in an experiment can be increased considerably (by a factor $\sim 2$) by placing the corresponding experimental setup about 1 m above the UCN guide from the reactor. This effect has an important impact on the layout of UCN sources with solid $^2H_2$ converters and experimentally supports the design used in ref. [43]. iv) Though expected from, *e.g.*, deceleration in neutron optics [44] and measurements of the absorption cross-sections at very low energies [45], this experiment confirms the recent first experimental verification of neutron acceleration by the material optical potential of a solid $^2H_2$ UCN converter [40]. v) The experimental method described here is very well suited, *e.g.*, for measurements of the temperature dependence in UCN production and for the necessary optimization of the UCN yield as a function of the source thickness. vi) It is demonstrated that the new superthermal neutron source with a solid $^2H_2$ UCN converter provides also "very cold neutrons" for experiments. These neutrons have velocities slightly above the UCN velocity range, *i.e.* with $7\,\mathrm{m/s} < v_\mathrm{n} < 25\,\mathrm{m/s}$ and are to our knowledge so far only available at the ILL in Grenoble.

This work was performed at the TRIGA Mark II reactor of the Johannes Gutenberg University in Mainz. It was supported by the DFG cluster of excellence Origin and Structure of the Universe (www.universe-cluster.de), by the DFG under the contract number Pa 762/3-1 (3-2), He 2308/2-1 (2-2), and GZ:436RUS17/107/06. Financial support from the Johannes Gutenberg-Universität Mainz in the framework of the Forschungsfonds is gratefully acknowledged. We thank H.-O. Kling, J. Breuel, A. Schmidt, and H.-M. Schmidt from the TRIGA reactor crew for their tireless help during the experiment and the efficient support from E. Gries in providing the liquid helium. The UCN detector was purchased from A. Strelkov, JINR, Dubna, Russia.

## References

1. Y.B. Zel'dovich, Sov. Phys. JETP **9**, 1389 (1959).
2. V.I. Lushikov *et al.*, JETP Lett. **9**, 23 (1969).
3. A. Steyerl, Phys. Lett. B **29**, 33 (1969).
4. V.K. Ignatovich, *The Physics of Ultracold Neutrons, Oxford Series on Neutron Scattering in Condensed Matter*, Vol. **5** (Clarendon Press, Oxford, 1990).
5. F. Atchison *et al.*, Phys. Lett. B **625**, 19 (2005).
6. T. Brys *et al.*, Nucl. Instrum. Methods Phys. Res. A **550**, 637 (2005).
7. C.A. Baker *et al.*, Phys. Rev. Lett. **97**, 131801 (2006).
8. S. Arzumanov *et al.*, Phys. Lett. B **483**, 15 (2000).
9. A. Serebrov *et al.*, Phys. Lett. B **605**, 72 (2005).
10. V.V. Nesvizhevsky *et al.*, Nature **415**, 6869 (2002).
11. R. Golub, J.M. Pendlebury, Phys. Lett. A **62**, 337 (1977).
12. C.R. Brome *et al.*, Phys. Rev. C **63**, 055502 (2001).
13. Y. Masuda *et al.*, Phys. Rev. Lett. **89**, 284801 (2002).
14. C.A. Baker *et al.*, Phys. Lett. A **308**, 67 (2003).
15. R. Golub, K. Böning, Z. Phys. B **51**, 95 (1983).
16. A. Saunders *et al.*, Phys. Lett. B **593**, 55 (2004).
17. C.L. Morris *et al.*, Phys. Rev. Lett. **89**, 272501 (2002).
18. F. Atchison *et al.*, Phys. Rev. C **71**, 054601 (2005).
19. I. Altarev *et al.*, www.kernchemie.uni-mainz.de/Dateien/a18_05.pdf.
20. F. Atchison *et al.*, Phys. Rev. Lett. **95**, 182502 (2005).
21. A. Steyerl *et al.*, Phys. Lett. A **116**, 347 (1986).
22. K. Eberhardt, A. Kronenberg, Kerntechnik **65**, 263 (2000).
23. G. Hampel *et al.*, Int. J. Nucl. Power **51**, 5 (2006).
24. H. Menke *et al.*, Kerntechnik **17**, 6 (1975).
25. A. Frei *et al.*, Eur. Phys. J. A **34**, 119 (2007).
26. Z.-Ch. Yu *et al.*, Z. Phys. B **62**, 137 (1986).
27. C.-Y. Liu *et al.*, Phys. Rev. B **62**, R3581 (2000).
28. E. Fermi, Ric. Sci. **7**, 13 (1936).
29. E. Fermi, W.N. Zinn, Phys. Rev. **70**, 103 (1946).
30. E. Fermi, L. Marshall, Phys. Rev. **71**, 666 (1947).
31. R. Golub, D.J. Richardson, S.K. Lamoreaux, *Ultra-Cold Neutrons* (Adam Hilger, Bristol, 1991).
32. I. Altarev *et al.*, Nucl. Instrum. Methods Phys. Res. A **578**, 450 (2007).
33. P. Fierlinger *et al.*, Nucl. Instrum. Methods Phys. Res. A **557**, 572 (2006).
34. F. Atchison *et al.*, Phys. Lett. B **642**, 24 (2006).
35. F. Atchison *et al.*, Nucl. Instrum. Methods Phys. Res. B **260**, 647 (2007).
36. G. Zsigmond *et al.*, Nucl. Instrum. Methods Phys. Res. A **529**, 218 (2004).
37. http://www.hmi.de/projects/ess/vitess/.
38. I. Altarev *et al.*, ILL Experimental Report, Experiment Test-939 (2005) unpublished.
39. A. Pichlmaier *et al.*, ILL proposal 3-14-213 (2006) unpublished.
40. I. Altarev *et al.*, Phys. Rev. Lett. **100**, 014801 (2008).
41. W. Klein *et al.*, AIP Conf. Proc. **596**, 193 (2001).
42. F. Atchison *et al.*, Phys. Rev. C **74**, 055501 (2006).
43. F. Atchison *et al.*, to be published in *ICANS-XVIII Proceedings, Donguan, Guangdong, PRC (2007)*.
44. A.I. Frank *et al.*, JETP Lett. **84**, 105 (2006).
45. H. Rauch *et al.*, Phys. Rev. Lett. **83**, 4955 (1999).